CHEMISTRY OF MATERIALS

pubs.acs.org/cm

Article

Thermodynamic Silver Doping of Core/Shell Colloidal Quantum Wells Imparted with Paramagnetic Properties Emitting at Near-Infrared

Farzan Shabani, Muhammad Ahmad, Satish Kumar, Savas Delikanli, Furkan Isik, Arinjoy Bhattacharya, Athos Petrou, and Hilmi Volkan Demir*

Cite This: *Chem. Mater.* 2023, 35, 4159–4170

Read Online

ACCESS | Metrics & More | Article Recommendations | Supporting Information

ABSTRACT: Two-dimensional (2D) core/shell nanoplatelets (NPLs) synthesized via the hot-injection method provide excellent thermal and chemical stability for high-temperature doping, where an expanded and flexible lattice is required. Here, a thermodynamic approach toward silver doping of these NPLs is proposed and demonstrated, which previously proved to be challenging due to the fast self-purification of the dopants with the introduction of the shell. Maintaining the doping procedure in the reversible regime ensured the integrity of the NPLs and allowed a high level of doping; however, the equilibrium condition is further complicated by environmental factors that affect the chemical activity of the cations and the surface composition of the NPLs. Two main deterioration mechanisms in the irreversible regime were observed: ZnS-shelled NPLs suffered preferential etching, while CdS-shelled NPLs underwent cleavage and fragmentation. Alloying of the shell minimized both mechanisms for CdZnS-shelled NPLs and preserved the metastable state of the NPLs, including their 2D shape and crystalline structure. Distribution of silver ions in the lattice of the NPLs directly affected the recombination dynamics and enabled fine-tuning of the near-infrared emission beside the exciton confinement. These silver-doped CdZnS-shelled NPLs are shown further to exhibit enhanced paramagnetic properties with Zeeman splitting and Brillouin-like bound-exciton polarization as a function of the magnetic field, critical for spintronic applications.

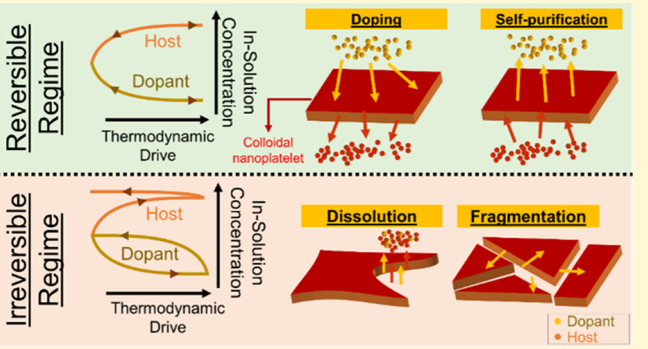

INTRODUCTION

Two-dimensional (2D) colloidal quantum wells (CQWs), also known as nanoplatelets (NPLs), have been the subject of intense studies during the past few decades because of their extraordinary optical properties compared to their spherical-shaped counterparts, the colloidal quantum dots. These NPLs demonstrate enhanced properties due to their atomically flat surface and anisotropic shape, which results in giant oscillator strength,[1] larger absorption cross-section,[2] and excellent photoluminescence quantum yield (PLQY).[3] These properties are highly desirable for optoelectronic applications ranging from light-emitting diodes and lasers to photocatalysts.[4−13] Because of their finite and atomically precise thickness, the emission spectrum of the NPLs is only tunable between discrete energy levels that limit their applications. However, in recent years, developing different strategies have overcome this problem to a large extent. Various electronic heterostructures of type-I and type-II core/crown or core/shell, alloying, and doping of the NPLs have enabled fine-tuning of their emission spectrum and even extended their emission beyond their bulk band gap energy values.[14−18] In particular, doping of the NPLs with transition metals has not only served as a way of emission tuning but also opened up the possibilities of imparting magneto-optical and magneto-electronic properties.[19−22] Due to the non-zero magnetic moment of the dopant ions, these magnetically doped nanocrystals (NCs) demonstrate two orders of magnitude higher Zeeman splitting than the non-magnetic ones,[23] which pave the way for applications such as magneto-optical gating,[24] spin filtering,[25] spintronics,[26] and charge engineering.[27]

Doping of group II−VI NCs with isovalent manganese atoms has long been under extensive investigation and has produced a rich literature.[28,29] Copper and, to a lower extent, silver have also been investigated as heterovalent dopants, with their emissions extending to 1100 nm.[30] So far, there have been two main methods of doping: first, in situ doping or else

Received: January 10, 2023
Revised: May 15, 2023
Published: May 29, 2023

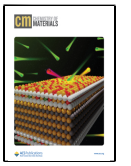

known as kinetically controlled doping, in which the dopant ions are incorporated during the nucleation and growth of the NCs and stay there as a result of a metastable thermodynamic condition.[31] Second, post-doping, also known as thermodynamically controlled or diffusion-controlled doping, in which the dopant ions are introduced to previously synthesized NCs and diffuse into the structure.[32,33] Incorporating dopant ions deep into the volume of the NCs through post-doping is a challenging process, as these ions with different ionic radii, charges, and coordination numbers are not favorable to form stable interstitial or substitutional sites. Moreover, the diffusion constant of these ions may be too low due to the hindrance from the lattice or insufficient chemical gradient.

Previously, it was shown that Cu and Ag impurities can replace the host Cd ions in the crystalline lattice sites through cation exchange, where the dopant ions diffuse interstitially[34] or via surface or bulk vacancies into the structure and substitute the Cd ions in the lattice.[35] For both of the proposed mechanisms, the chemical activities (μ) of the dopant ions in the solution and the lattice play a central role in the doping level. Especially at high doping temperatures, where the lattice is flexible enough, chemical activity determines the diffusion direction and equilibrium concentration of the dopant, which in many cases result in the depletion of the dopant ions in a reverse exchange reaction known as self-purification.[36,37] A mere increase in the dopant precursor concentration is also not the best strategy, as it can cause re-nucleation and destabilization of the original NCs and lead to the formation of unwanted species.

Recently, 2−6 monolayer (ML) CdSe NPLs have been successfully doped with silver through the post-doping process. Moreels's group demonstrated high silver doping affinity even at 0 °C with the silver acetate precursor quenching the band-edge emission.[38] Separately, Dufour et al. looked into the Ag-activated states in CdSe NPLs and concluded that the sub-band energy level of doped NPLs remains fixed in contrast to QDs.[17] While post-silver-doping of 2−6 ML CdSe NPLs seems feasible, putting a shell with a different composition has been a pending challenge because it causes re-emergence of the band-edge emission after deposition of the shell.[38] This problem is usually attributed to the self-purification of the NCs, possibly during the shell deposition process.[28,32,39−42]

Here, we propose and demonstrate a high-temperature thermodynamic approach toward silver doping of core/shell NPLs with different shell compositions. This method allows us to dope the core/shell NPLs in a high dopant regime, which previously proved to be challenging due to self-purification and the long diffusion distance imposed by the extra layers of shell. We investigate the effect of different shells of ZnS, CdS, and alloyed CdZnS on the integrity of the NPLs during the high-temperature doping and demonstrate that the composition of the shells strongly affects the destruction process of the NPLs. NPLs with the tendency to form silver islands on the surface would undergo etching and dissolution in the irreversible doping regime. In contrast, those with no affinity of surface silver islands would experience fragmentation and segmentation. Since retaining the doping process in the reversible regime is important, NPLs with an alloyed CdZnS shell exhibit prolonged doping resistance, and they best preserve their integrity at high temperatures. The recombination dynamics were very sensitive to the end-product-doped NPLs, where the distribution of silver ions strongly determines the recombination channels and lifetimes. The silver-doped NPLs demonstrate paramagnetic properties, with the bound excitons possessing a negative Brillouin-like dependence in the presence of a magnetic field and a positive Zeeman splitting. Strongly affected by the doping dynamics, NPLs with higher doping tendencies showed enhanced paramagnetic properties.

EXPERIMENTAL SECTION

Detailed information about the materials and synthesis routes of cadmium myristate, CdSe core and CdSe/CdZnS core/shell NPLs are provided in the Supporting Information. The synthetic procedure for doping the core/shell NPLs with different shell compositions is described below. The optical properties of the doped NPLs, including PL spectra, absorption profile, PLQY and time-resolved photoluminescence (TRF), were measured. Further characterizations have been done using transmission electron microscopy (TEM) imaging, X-ray photoelectron spectroscopy (XPS), X-ray diffraction analysis (XRD), magnetic circularly polarized luminescence (MCPL) and inductively coupled plasma mass spectrometry (ICP-MS), details of which can be found in the Supporting Information.

Synthesis of Ag-Doped CdSe/$Cd_xZn_{1-x}S$ Core/Shell NPLs. The doping procedure was performed on the preprepared core/shell NPLs with different shell compositions (details of the synthesis of core/shell NPLs are presented in the Supporting Information). First, a silver precursor was prepared by dissolving 0.3 mmol of $AgNO_3$ in a mixture of 150 μL of TOP and 18 mL of ODE. In a typical synthesis, 1 mL of core/shell NPLs (equivalent to a quarter of the total core/shell NPLs synthesized in the previous step) and 3.5 mL of ODE were put in a three-neck flask and degassed at room temperature for 1.5 h. The solution was further degassed at 90 °C for 30 min to ensure that hexane and other volatile spices were removed. Then, the flask was flushed with argon gas, and the temperature was increased to 160 °C. The silver precursor was injected at an injection rate of 2.5 mL/h. After injection of 1 mL of the precursor, the temperature was increased with 10 °C increments and a retention time of 1 min for each step. The solution was quenched in water at 240 °C and diluted with 5 mL of hexane. Doped NPLs were precipitated by adding extra ethanol and centrifugation and redispersed in hexane for further use.

RESULTS AND ANALYSIS

A fully thermodynamically controlled doping process requires the dopant atoms to diffuse into the lattice upon increasing the driving force and diffuse out when the driving force is reversed without disturbing the structure. Figure 1 is a schematic of reversible and irreversible doping processes. The concentration of dopant (host) atoms at the beginning of the process is at its highest (lowest) point inside the medium solution (excluding the NPLs). As doping of the NPLs proceeds, the dopant concentration will decrease, and at the same time, the host concentration will increase in the solution as a result of the host-dopant exchange reaction. The driving force of doping is a sum of complex interweaved factors, including concentration and temperature. For example, intuitively increasing the dopant concentration should enhance the doping level; however, as was previously shown, increasing the dopant concentration reduces the doping affinity after a certain point (one reason can be the preference for nucleation over doping).[43] Or, as we will show, increasing the temperature would initially increase the doping level in the NPLs, followed by a decrease from a certain point on. A reversible (or non-destructive) doping requires the host and dopant atoms to return to their initial positions through reverse exchange reaction and diffusion without affecting the structure (Figure 1a). The in-solution concentration of the host and dopant atoms and NPLs will be the same as the beginning in this process. On the other hand, an irreversible (or destructive)

https://doi.org/10.1021/acs.chemmater.3c00058
Chem. Mater. 2023, 35, 4159−4170

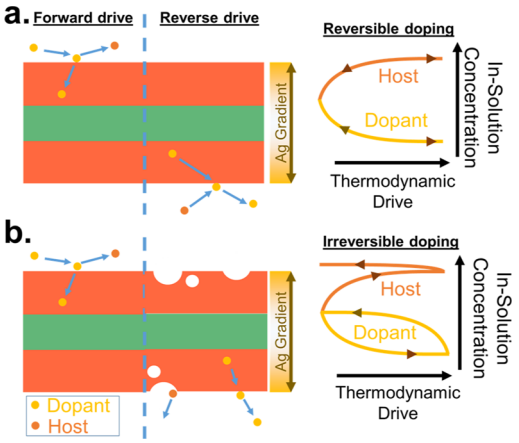

Figure 1. Schematics of (a) reversible non-destructive doping and (b) irreversible destructive doping. Under both regimes, increasing the driving force would decrease the in-solution dopant concentration and increase the host concentration. However, for a reversible process, the NPLs retrieve their original composition upon a decrease in the driving force through a reverse exchange reaction, while for an irreversible process, the NPLs cannot regain their initial form (composition, shape, etc.).

doping process is one that upon reversing the driving force, the dopant ions diffuse out of the structure, but the process is not complemented with a reverse exchange reaction, or worse, it may be accompanied by dissolution or etching of the crystal. In this destructive process, the in-solution concentration of the dopant and host atoms will increase, while the number of NPLs may decrease or NPLs may end up partially damaged (Figure 1b). One important aspect of this classification is that for most of the doping processes, this is the increase in the forward driving force (temperature, dopant concentration, etc.), which may hit a no-return point where the equilibrium completely changes in favor of some other phenomena such as dissolution, re-nucleation, etching, etc. In that sense, the most important factor is to keep the doping process in the reversible regime and then kinetically trap the dopant atoms in the lattice. Once the equilibrium is disturbed, the chance of doping and self-purification decreases, and the NPLs may deteriorate through a destructive and irreversible process.

NPLs with a hot-injection (HI) shell are known for their high-temperature stability in comparison with the room-temperature grown shell NPLs, traditionally formed through the colloidal atomic layer deposition (c-ALD) technique.[44,45] Conducting our post-doping synthesis at high temperatures, these NPLs are the best choices as they can expand their crystalline structure, providing a fluid enough lattice while maintaining their integrity. To tune the shell thickness, the initial amount of anion and cation precursors during HI shell growth was kept constant, and the thickness of the shell was carefully controlled by varying the growth time (see the Methods, Supporting Information).

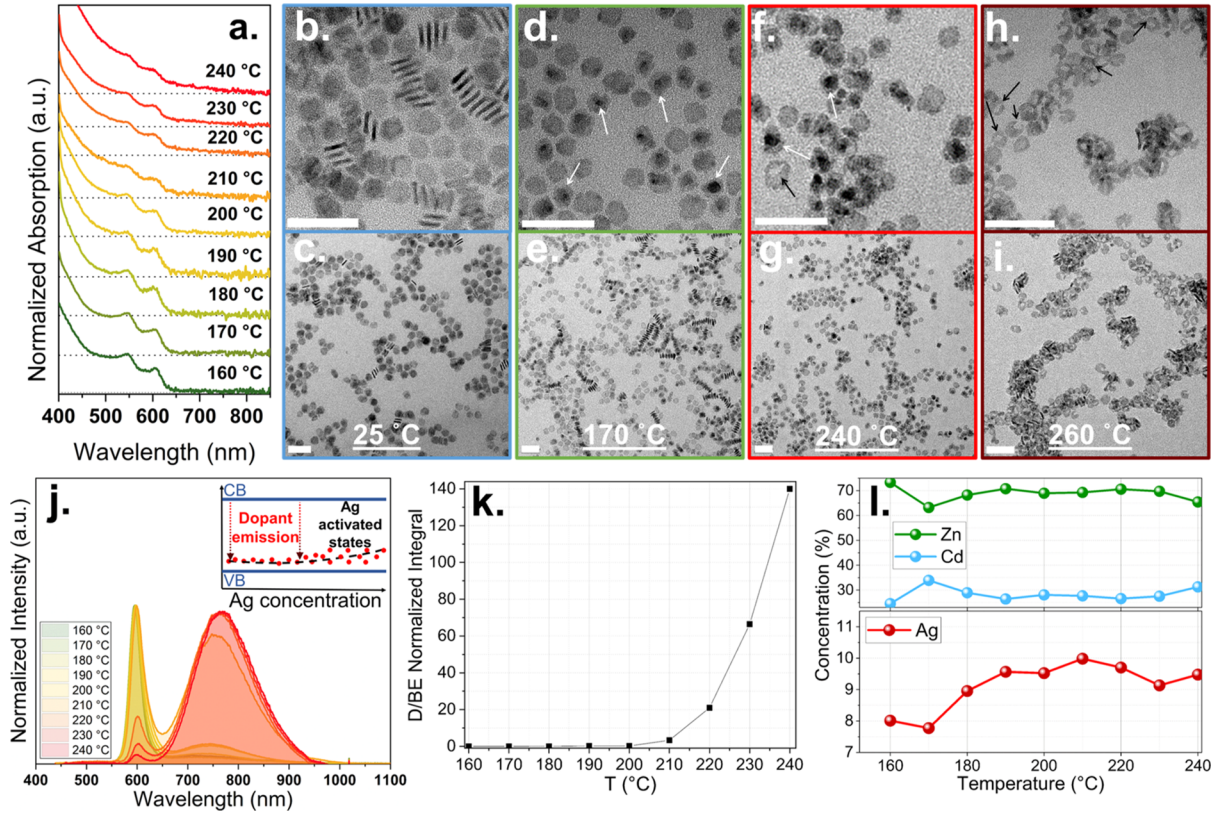

Figure 2. (a) Absorption profile for aliquot samples of Ag/CdSe/ZnS core/shell NPLs after complete injection of Ag precursor at 160 °C, taken while the doping temperature was increased from 160 to 240 °C. TEM images of the samples at four different temperatures of (b,c) 25 °C (before the injection of the doping precursor), (d,e) 170, (f,g) 240, and (h,i) 260 °C. Scale bars are 50 nm. The black and white arrows show the silver islands and etching sites on the NPLs, respectively. (j) Emission spectra of the aliquot samples corresponding to the NPLs in (a). The inset is a schematic showing the dependency of the position of the mid-gap states on the Ag concentration. (k) Evolution of dopant/band-edge emission ratio with increasing temperature. (l) ICP−MS analysis of Ag concentration.

https://doi.org/10.1021/acs.chemmater.3c00058
Chem. Mater. 2023, 35, 4159−4170

For the first set of our doping experiments, we used CdSe/ZnS core/shell NPLs with band-edge emission at 596 nm, indicating a relatively thin shell with 4 ML of ZnS on each side (absorption and PL spectra are provided in Figure S1).[46] The evolution of the absorption spectra of the CdSe/ZnS core/shell NPLs after adding 1 mL of Ag precursor is demonstrated in Figure 2a. For all temperatures ranging from 160 to 240 °C, the first and second excitonic peaks associated with the heavy and light hole transitions remain distinct, indicating the intact 2D shape of the NPLs. As the doping temperature increases, the charge-transfer (CT) excited state starts to appear due to the fast localization of the hole, which nominally oxidizes Ag^{+} to Ag^{2+} and makes strong bonding with electrons in the conduction band, similar to previous reports on copper-doped QDs and CdSe only-core NPLs.[30,38,47] The CT state is not obvious at lower temperatures; however, the emission spectra (Figure 2j) develop dopant emission characteristics from the initial temperature of 160 °C, which means dopant ions diffuse into the structure even at low temperatures.

We calculated the dopant to band-edge (D/BE) emission fraction simply by dividing the area below the dopant emission peak to the band-edge emission peak. The evolution of D/BE emission versus doping temperature, shown in Figure 2k, demonstrates a sudden increase at temperatures above 210 °C. However, the band-edge emission does not completely fade away even at high doping temperatures. It is important to stress that introducing silver to the NPLs at room temperature did not yield any meaningful dopant emission (Figure S2), despite the previous reports in the literature for the core-only NPLs.[17,38] Figure 2l shows the concentrations of silver, cadmium, and zinc in the NPLs determined via ICP−MS. Ag concentration increases monotonously with increasing the temperature; however, the evolution of Ag concentration demonstrates two unusual features: First, even at a relatively lower temperature of 160 °C, the core/shell structure is already heavily doped with silver. This behavior is unlike the other Ag-doped core/shell samples in this study. Moreover, the increase in the concentration continues up until 210 °C, where it reaches its maximum of 10% and then declines at higher temperatures. On the other hand, Zn and Cd keep their concentrations after the initial stage and only fluctuate around that concentration. The later drop in Ag concentration shows that the silver ions are moving out of the lattice. There are multiple factors governing over this anomalous behavior. First, at increased temperature, the expanding crystalline structure of the NPLs grants more freedom for atoms to diffuse in the lattice structure with a higher diffusion constant (D) scaling with $\propto \exp(-1/T)$.[48] Moreover, the silver ions residing in the interstitial or substitutional sites act as defects that disturb the homogeneity and purity of the crystalline structure. The equilibrium number of these defects in a crystalline structure also scales up with Arrhenius dependency over temperature.[48] Both factors should principally enhance the doping of the NPLs, but in fact the doping level is decreased. The reason for the shift in the diffusion direction of silver ions from populating the NPLs at a lower T to evacuating them at a higher T is not the solid solution's thermodynamic equilibrium but the higher solubility of the silver ions in the solvent. At the minuscule Ag concentration (3.5 mM), in which the synthesis has been carried out, a small shift in the salt-liquid solubility imposes a huge change on the thermodynamic equilibrium within the NPLs, which ultimately reverses the diffusion direction of the atoms and force them out of their inherent defect sites.

As can be seen in the TEM images (Figure 2b−i) of the samples obtained at different temperatures, the 2D shape of the NPLs is conserved until 240 °C. The NPLs underwent dissolution above this temperature, with almost all of them (at 260 °C) carved out from the center. The dissolution process has not caused any fragmentation of the NPLs, as the image does not show any size change of the NPLs. Moreover, it seems that even at lower temperatures, there are silver-rich islands on some of the NPLs (Figure 2d−g), which do not change in numbers significantly by increasing the temperature. Consistent with previous reports in the literature, when the concentration of the dopant ions exceeds a number, a silver metallic tip will form on the NPLs.[17] The TEM-EDS map of ZnS-shelled NPLs doped with Ag in Figure S3 shows that away from the islands, silver is distributed homogeneously on the NPLs. However, its concentration on the islands is much higher than in other regions, suggesting that the islands predominantly consist of silver. Also, the concentration of Cd on these islands is slightly higher, which indicates the Cd and Ag alloying. These islands are absent at 260 °C, suggesting that they are preferably detached and are partially accountable for NPLs shape instability.

Up until 240 °C, the share of dopant emission is increasing (Figure 2k), despite the decrease in the overall concentration of Ag (Figure 2l). This is due to the retention of silver inside the lattice structure that experiences difficulty to diffuse out in comparison to surface silver islands. The TEM images confirm this behavior, as the islands are the first silver-rich spots that are dissolved. At temperatures above 240 °C, the NPLs lose their entirety and the excitonic features fade away, as seen in their absorption profile in Figure S4. The band-edge and dopant emission peak wavelengths of the NPLs, presented in Figure S5, exhibit consistent red shift with increasing temperature. While the band-edge peak position is less sensitive to silver concentration (it only red-shifts from 596 to 602 nm), the dopant emission exhibits great sensitivity to the presence of silver and red-shifts from 729 nm to a maximum of 769 nm. The behavior is reasonable as the silver ions would not alter the size of the NPLs and hence would not affect the confinement and direct bandgap energy. However, silver ions populate the sub-band energy levels that introduce new conduction band-sub-band transition channels with lower energy. The very small red shift in the band-edge emission peak wavelength is probably due to the island formation of the NPLs at high temperatures, which produces a thickness distribution at mid-range temperatures and increases the full width at half-maximum (FWHM, Figure S5).

With the same 4 ML CdSe core, changing the thin shell of ZnS with CdS should not change the doping process substantially; however, CdSe/CdS core/shell NPLs follow completely different doping dynamics. For the second core/shell NPL doping, we used CdSe/CdS core/thin-shell NPLs emitting at 652 nm (Figure S1c), corresponding to approximately 4−5 ML of CdS shell on each side.[49] The red shift in the original band-edge emission wavelength from ZnS-shelled to CdS-shelled NPLs is mainly due to the smaller valance band offset between CdSe and CdS than ZnS and partially because of thicker core/shell NPLs.[50] The first difference from the case of ZnS-shelled NPLs after the introduction of Ag precursor is the decreased number of metallic islands (Figure 3a−c). These islands are probably the

https://doi.org/10.1021/acs.chemmater.3c00058
Chem. Mater. 2023, 35, 4159−4170

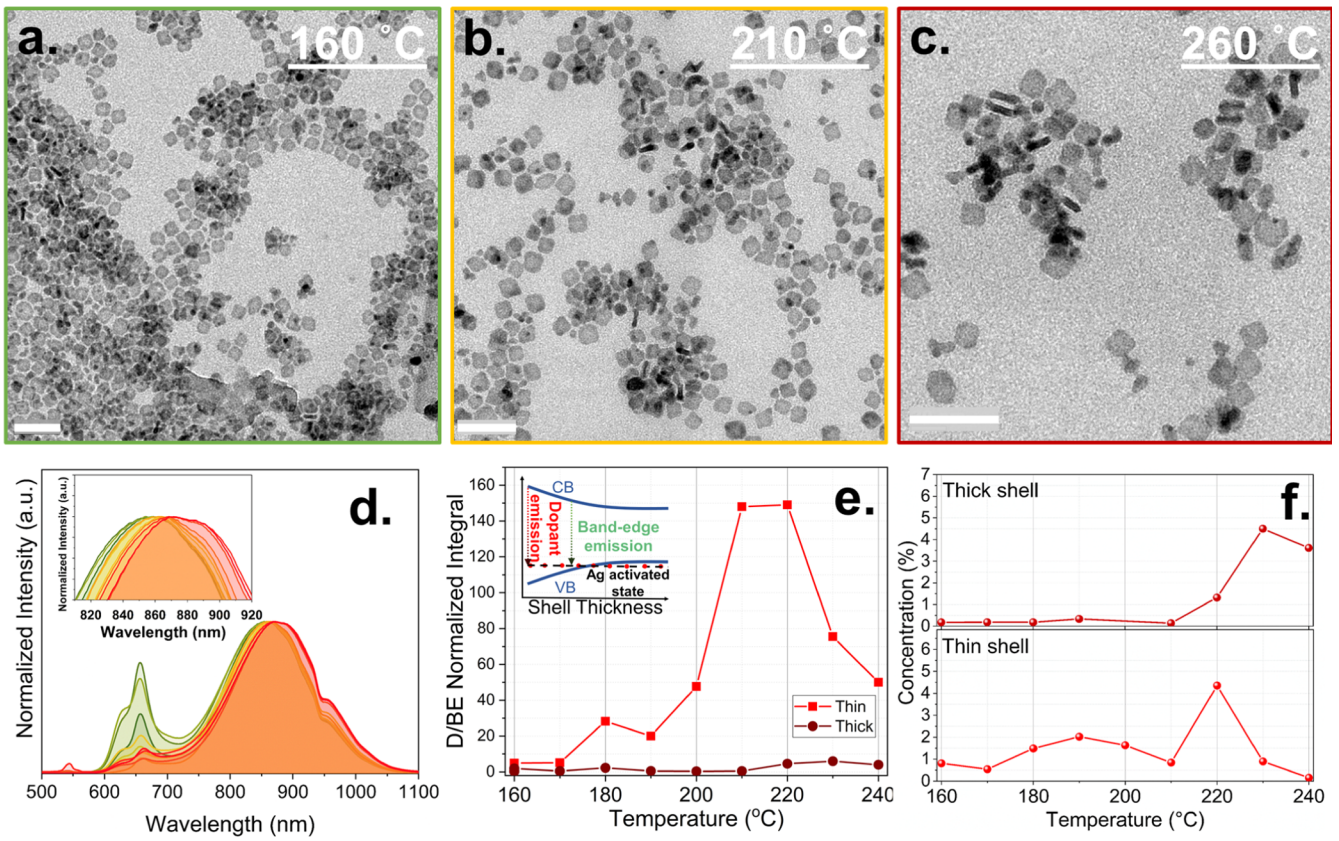

Figure 3. TEM images of CdSe/CdS core/shell NPLs at (a) 160 °C before the injection of Ag precursor and (b,c) at 210 and 250 °C, respectively, after the injection of Ag precursor. Scale bars are 50 nm. (d) Evolution of PL spectra of Ag/CdSe/CdS core/shell NPLs within the temperature range of 160 (green line) to 240 °C (red line). The inset follows the red shift in the dopant emission with increasing the temperature. (e) D/BE emission ratio. The inset is a schematic showing the decrease in the band-edge with increasing the shell thickness. The thick-shelled samples show negligible dopant emission as the Ag-activated states are no longer inside the bandgap. (f) Ag concentration measured via ICP−MS from aliquots taken during the synthesis. For thick-shelled samples, the core/shell synthesis was prolonged and its emission was red-shifted compared to the thin-shelled NPLs due to the confinement relaxation.

reason for the extra-high Ag concentration for ZnS-shelled NPLs in comparison to CdS-shelled NPLs, especially at low temperatures. Another fundamental difference between these two sets of NPLs is the destruction mechanism at high temperatures. While for ZnS-shelled NPLs, some holes form at temperatures above 240 °C due to the dissolution of NPLs from preferred silver island sites, CdS-shelled NPLs demonstrate fragmentation and segmentation at higher temperatures. The fragmented NPLs are obvious at 260 °C in Figure 3c. Both sets of NPLs do not tolerate high doping temperatures and disintegrate, but for ZnS-shelled NPLs, the process involves preferred dissolution sites provided by Ag islands rather than the fast fracturing of CdS-shelled NPLs.

The evolution of photoluminescence spectra in Figure 3d sheds more light on the doping kinetics of the CdS-shelled NPLs. First, even at 160 °C, the share of dopant emission exceeds the band-edge emission and increases continuously until 220 °C. However, above 220 °C, the band-edge emission again starts to gain prominence, as seen in Figure 3e (thin). The behavior is unlike the CdSe/ZnS core/shell NPLs, where in spite of a much higher initial Ag concentration, the dopant emission remains negligible until 200 °C, and also after decreasing the Ag concentration, no resurgence of the band-edge emission is observed. This different behavior indicates a higher diffusion coefficient of Ag ions in the lattice of CdSe/CdS core/shell NPLs that requires less thermal energy and can enter and exit the lattice much easier. For ZnS-shelled NPLs, much of the silver concentration is coming from the surface islands, but for CdS-shelled NPLs, Ag has diffused more effectively at low temperatures. The higher diffusion coefficient dictates the faster dopant emission emergence and, at the same time, leads to a higher self-purification rate and the NPLs recovery at high temperatures when the doping driving force is reversed.

To fully understand the doping process of these NPLs, we also synthesized another set of CdSe/CdS core/shell NPLs with a thicker shell. These NPLs, designated as thick, demonstrate weaker sensitivity in their emission spectra to silver concentration, and their D/BE ratio does not exceed even 10 at all temperatures (Figure 3e), while their concentration of silver is increasing similar to the thin-shelled NPLs. Figure 3f demonstrates the concentration of Ag in the thin-shelled NPLs, which is in line with the PL spectra. A sudden increase in the Ag concentration at 220 °C is followed by a decrease at higher temperatures, similar to the ZnS-shelled NPLs, meaning self-purification is also in process. Ag concentration in thick-shelled NPLs undergoes the same sudden increase at 230 °C and then again decreases (Figure 3f). The higher doping/self-purification equilibrium temperature indicates that the diffusion time and distance required for Ag ions in thick-shelled NPLs are increased, and consequently, the whole process is shifted to higher temperatures. More

https://doi.org/10.1021/acs.chemmater.3c00058
Chem. Mater. 2023, 35, 4159−4170

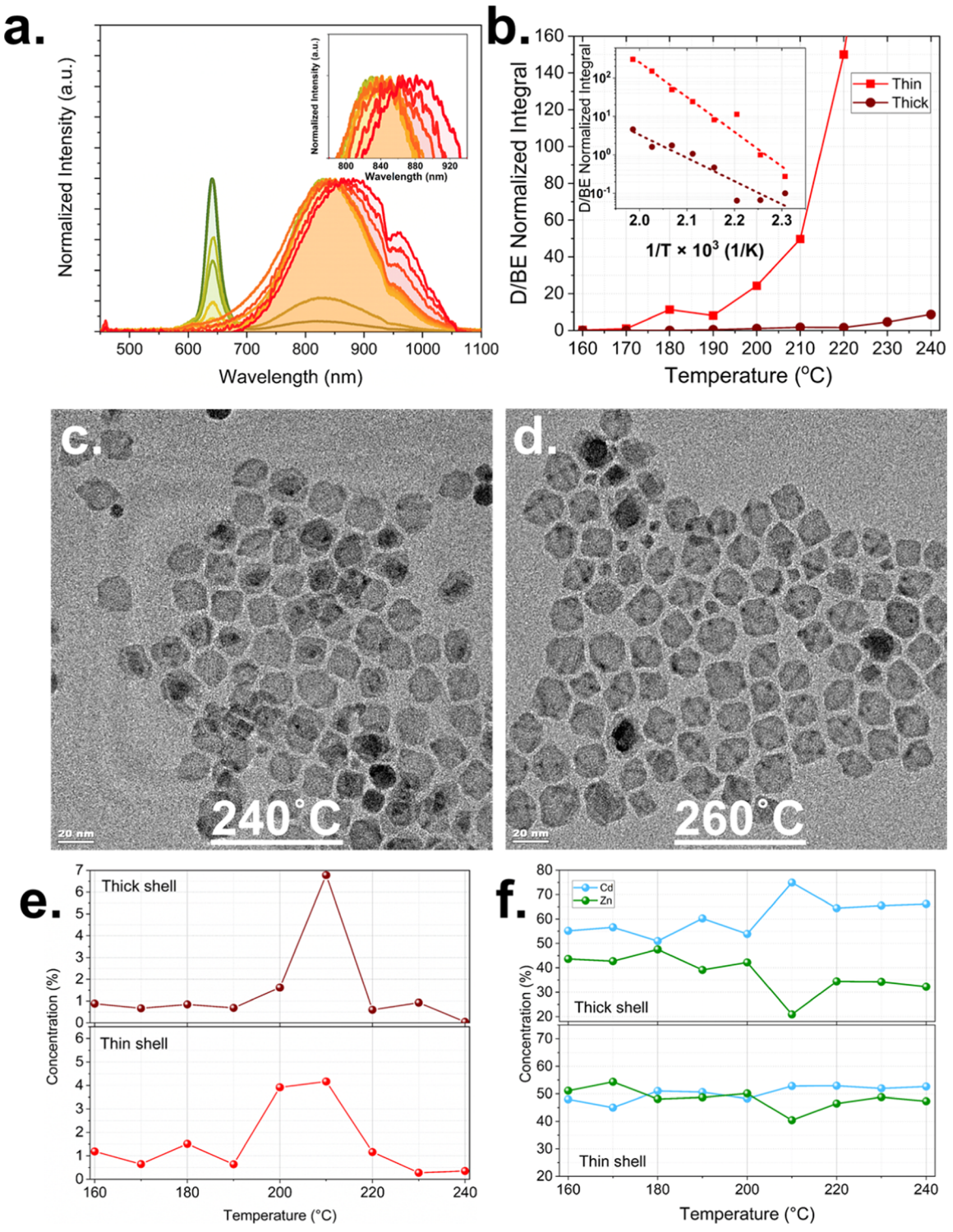

Figure 4. (a) PL emission spectra of CdSe/CdZnS core/shell NPLs after injection of the Ag precursor from 160 °C (green line) to 240 °C (red line). The inset follows the red shift of dopant emission with increasing temperature. (b) D/BE emission ratio for thin- and thick-shelled NPLs. The inset is the Eyring plot for the same data. (c,d) TEM images of the samples for thin CdZnS-shelled NPLs taken at 240 and 260 °C, respectively. (e) Concentration of Ag and (f) Cd and Zn for CdZnS-shelled samples obtained via ICP−MS analyses.

importantly, increasing the shell thickness decreases the direct bandgap energy of the NPLs, and resultantly, decreases the chance of the mid-gap states to form inside the bandgap. These thick-shelled NPLs show a minor sign of dopant emission. This observation also confirms previous reports where the silver-activated states do not depend on confinement and thickness.[17] The dopant-emission peak position for thin-shelled NPLs in Figure 3d (summarized in Table S1) exhibits consistent red shift from 852 to 862 nm. For the CdS-shelled NPLs, the peak position is much deeper in the red side of the spectra compared to the ZnS-shelled NPLs with a maximum of 767 nm. Also, the red shift is merely 10 nm, in comparison to 38 nm for ZnS-shelled NPLs. Both of these differences are because of the much lower conduction band offset of CdS-

https://doi.org/10.1021/acs.chemmater.3c00058
Chem. Mater. 2023, 35, 4159−4170

shelled NPLs, which decreases the mid-gap charge transfer energy. More importantly, as the red shift in the dopant emission exhibits a significant decrease, there must be a saturation point where, for tighter bandgaps, the silver mid-gap state would not fall in between the valance and conduction bands. For this reason, our thick CdS-shelled NPLs did not demonstrate the same level of D/BE emission. To cross-examine this hypothesis, we synthesized extra-thick CdS-shelled NPLs and tried to dope them using the same procedure. The PL evolution of these NPLs with temperature is demonstrated in Figure S6a. For all of the temperatures, the share of dopant emission is less than the band-edge emission (Figure S6b), and increasing the temperature only seems to direct it toward zero-level.

So far, it has been shown that ZnS-shelled NPLs collapse during high-temperature doping because of the formation of silver islands that later act as sweet etching spots, while for CdS-shelled NPLs, the fragmentation is the leading cause of destruction. For the third set of our experiments, NPLs with thin CdZnS alloyed shell were synthesized, and the same doping procedure was performed. The evolution of the PL spectra with increasing the doping temperature is shown in Figure 4a (summarized in Table S2). The original band-edge emission peak wavelength of CdZnS-shelled NPLs is between those of ZnS- and CdS-shelled NPLs (Figure S1d). At a low temperature of 160 °C, the dopant emission is completely absent, while above 220 °C, the dopant emission overrides the band-edge emission (Figure 4b, thin). The behavior is unlike the previous doped NPLs, while drawing some similarities with each of them. The TEM image of these NPLs at 240 °C in Figure 4c indicates that the number of silver islands is higher than that of CdS-shelled NPLs and lower than that of ZnS-shelled NPLs. The D/BE emission goes to infinity (Figure 4b, thin), which means that Ag ions effectively diffused into the lattice and the dopant emission is not only the result of the islands on a sparse number of NPLs. The TEM image of doped NPLs at 260 °C, with no cleaning after sampling, is shown in Figure 4d. Interestingly, for these overheated NPLs, fragmentation and dissolution exist, but both of them are inhibited to the highest degree. Dissolution is minimized, and the fewest of the NPLs are broken and cleaved. If the broken pieces are not considered, the lateral size distribution of the NPLs is almost the same, which indicates that small pieces are part of the broken NPLs that do not exist anymore. As was expected, the silver islands are completely wiped out due to their high-temperature instability that was observed for ZnS-shelled NPLs.

The PLQY of the CdZnS-shell NPLs was measured at different temperatures and is shown in Figure S7. At lower temperatures, the PLQY is at its highest, and at higher temperatures, it drops, probably due to the severe reaction condition. The high-temperature doped NPLs possess a high PLQY of 44%, with all the share of emission coming from the dopant. The PLQY goes up to a maximum of 56% for the partially doped NPLs with 90% of the PL coming from the dopant. The crystalline structure of the CdSe/CdZnS core/shell NPLs was examined through XRD measurements before and after doping (Figure S8). Doped NPLs showed no significant change in the diffraction peak positions, indicating the preservation of the original zinc blende crystalline structure. There was no trace of characteristic peaks of either monoclinic or cubic Ag_2S and Ag_2Se to suggest nucleation of side products.[51] The XPS spectra of silver for doped CdSe/CdZnS core/shell NPLs in Figure S9 verifies successful doping of the NPLs with peaks at 367.88 and 373.88 eV corresponding to Ag $3d_{5/2}$ and Ag $3d_{3/2}$ orbitals, respectively. The unchanged S 2p and Se 3d XPS peak profiles and Ag 3d peaks suggest the silver ions sit in tetrahedral sites surrounded by four sulfide ions.[52,53]

For another ensemble of NPLs with thick CdZnS shell, the share of dopant emission did not increase substantially even at high temperatures (Figure 4b). However, if D/BE emission for thin- and thick-shelled NPLs is plotted on a semi-log scale (inset of Figure 4b), the increase in the dopant emission share follows similar behavior over temperature for both sets of NPLs. The absence or minimization of the dopant emission for thick-shelled NPLs happens as the silver mid-gap states are dropped out of the bandgap of the NPLs, as was shown for CdS-shelled NPLs. The linear behavior of D/BE in the semi-log plot may be an indication of the Arrhenius type of activation of the doped NPLs, where D/BE $\propto \exp(-1/T)$. The calculated slope for this linear fit (dash lines) for thin-shelled NPLs is 1.5 times higher than that of thick-shelled NPLs. This slope in the Arrhenius equation is related to the activation energy ($\propto \frac{-E_a}{RT}$, where E_a is the activation energy and R is the gas constant), which is unpredictably higher for thin-shelled NPLs than for thick-shelled NPLs. The higher E_a implies a slower process and probably less doping.

Figure 4e demonstrates the concentration of silver in both sets of CdZnS-shelled NPLs. Thin-shelled NPLs have a lower Ag concentration at their highest point than thick-shelled ones with a lower doping temperature threshold. In line with the results from D/BE emission, the higher activation energy is responsible for lower doping in the thin-shelled NPLs. This is also similar to the results in Figure 3e,f, where thick CdS-shelled NPLs are more doped than the thin-shelled NPLs but still possess low dopant emission. Thick NPLs provide more interstitial or substitutional sites with a deeper concentration gradient over their structure, which is necessary for any diffusion process. Figure 4f shows that, for both sets of NPLs, Zn is preferably more prone to give its position to silver at high temperatures, which is more pronounced for thick-shelled NPLs where Ag concentration is 1.5 times higher.

One common strategy in the colloidal synthesis of NCs is the introduction of long-chain carboxylic acid or amine, especially oleic acid (OA) and oleylamine (OLA), which act as ligands and enhance the optical properties and colloidal stability. In two experiments, we introduced OA and OLA at the end of the doping of CdZnS-shelled NPLs to investigate the effect of these ligands (details and results of the experiments can be found in the Supporting Information, Figures S10 and S11). Both sets of doped NPLs demonstrated re-emergence of the band-edge emission for short introduction times of ligands, probably due to self-purification, while the shape of the NPLs remained intact.

Alongside the spectral shift of the emission peak wavelength, heterovalent doping of the semiconductor NCs is known to alter the emission kinetics drastically. Here, three new sets of half-doped thin-shelled NPLs (having a dopant to band-edge PL peak intensity ratio equal to one) with three different shell compositions of ZnS, CdS, and CdZnS were prepared and their emission decays were measured via TRF spectroscopy. Figure 5a depicts the PL decay curves for these three samples, where each curve is fitted with a three-exponential function. It is known that even for near-unity core/shell NPLs reaching

https://doi.org/10.1021/acs.chemmater.3c00058
Chem. Mater. 2023, 35, 4159−4170

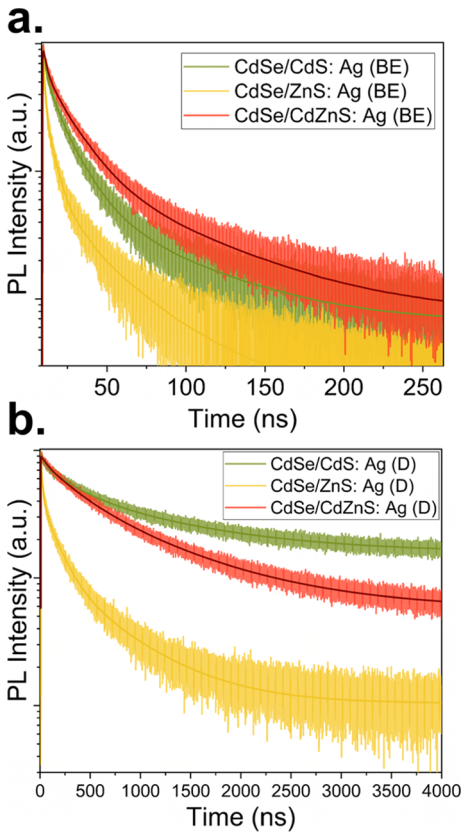

Figure 5. TRF decay curves of thin-shelled NPLs with respective heterostructures of CdSe/ZnS, CdSe/CdS, and CdSe/CdZnS core/shell. All three samples were half-doped with Ag, in which the dopant to band-edge PL peak intensity ratio equals one: (a) band-edge emission decay after doping and (b) dopant emission decay curve.

mono-exponential decay is not possible due to the existence of nonradiative recombination channels.[50] The samples exhibit band-edge recombination lifetimes (τ_{avg}) ranging from 4.0 to 15.4 ns, which is the characteristic lifetime of thin-shelled NPLs (details in Table S3a). The comparatively fastest recombination lifetime of ZnS-shelled NPLs is originated in its thinner shell, which results in a lower band-edge emission wavelength and closer proximity of the electron and hole (for comparison, see the absorption and emission spectra of the initial NPLs presented in Figure S1). Implementing Ag ions into the lattice opens up new channels for carrier trapping and consequently increases the recombination lifetime. Generally, a shorter recombination lifetime indicates fast nonradiative channels where trapped electrons on the surface of the NC recombine nonradiatively with holes.[54,55] We showed that ZnS-shelled NPLs are more prone to the nucleation of silver islands. These islands act as electron scavengers and accelerate electron trapping on the surface of NPLs. Moreover, ZnS-shelled NPLs undergo etching and carving, which in turn reduce the electron−hole distance. The maximum τ_{avg} for CdZnS-shelled NPLs is the result of both their higher stability and lower fast nonradiative channels of these NPLs. The dopant emission decay curves for all three samples demonstrate at least two orders of magnitude longer recombination lifetime (Table S3b), similar to previous reports in the literature.[56,57] For ZnS-shelled NPLs, it was shown that the PL emission has the highest energy with the least red shift for its dopant emission wavelength compared to the other two samples. The shortest τ_{avg} for its dopant emission is originated in the highest emission energy and, as a result, its shortest electron−hole recombination pathway. In accordance with the donor−acceptor pair (DAP) model, the distribution of the Ag mid-gap states implies that those electrons and holes that stand

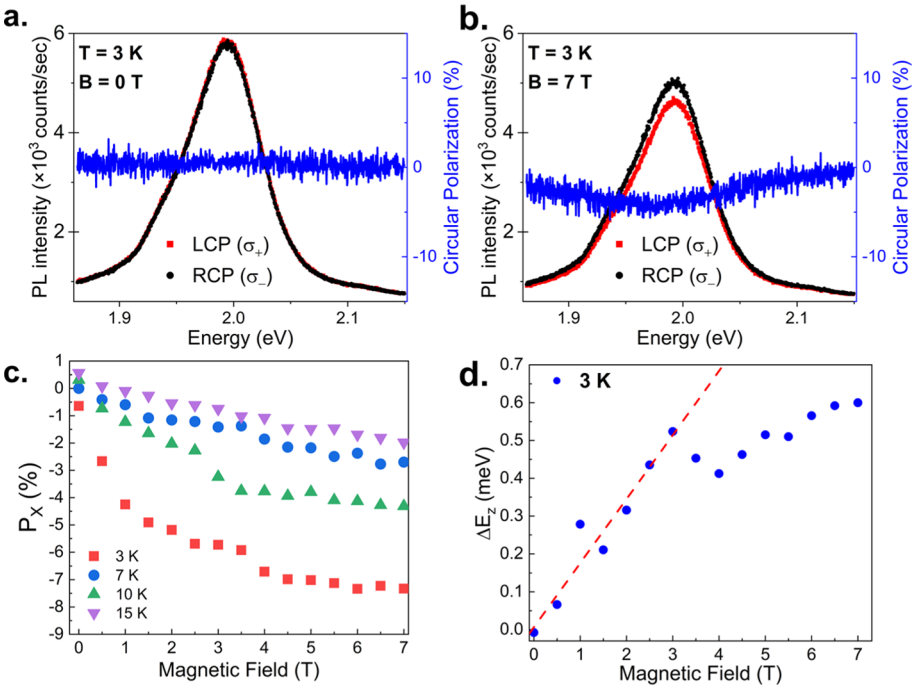

Figure 6. (a) RCP and LCP components of photoluminescence for partially silver-doped CdSe/CdZnS core/shell NPLs at 3 K and in the absence of a magnetic field. The circular polarization, shown in blue line, is almost zero in the band-edge emission vicinity. (b) Same measurement at an increased magnetic field of 7 T. The bound exciton feature, at energy P_X, demonstrates negative circular polarization. (c) P_X vs the magnetic field (B) for a temperature range from 3 to 15 K. (d) Bound exciton Zeeman splitting (ΔE_Z) as a function of B at T = 3 K.

https://doi.org/10.1021/acs.chemmater.3c00058
Chem. Mater. 2023, 35, 4159−4170

closer to each other are more affected by the Coulomb interaction and therefore recombine faster and produce higher PL quanta energy.[58,59]

Unlike isovalent dopants such as Mn, Ag^+ ions with a full d shell are capable of capturing the photoexcited holes from the valance band of the host material. The new Ag^{2+} ions possess an unpaired electron, which gives rise to a non-zero magnetic moment and can be detected through MCPL spectroscopy.[60] To observe the effect of Ag^+ ions on the magnetization, it is essential to keep the dopant content restricted so that the band-edge emission remains strong for the measurement.[19] Using our half-doped CdSe/CdZnS core/shell NPLs, the left circularly polarized (LCP, σ_+) and right circularly polarized (RCP, σ_-) components of the PL at the band-edge were measured at T = 3 K for magnetic fields (B) up to 7 T (Figure 6a,b). The temperature-dependent PL of these NPLs in the band-edge vicinity (Figure S12) exhibits emission peak broadening with decreasing temperature, attributed to the strain variation and interaction of band-edge excitons with the silver impurities. Defining circular polarization as $(I_+ - I_-)/(I_+ + I_-) \times 100$, where I_+ and I_- are the intensities of the σ_+ and σ_-, respectively, the polarization remains zero with no apparent feature for B = 0 T. With increasing magnetic field to 7 T, a negative value of polarization related to the bound excitons was observed. The bound exciton circular polarization (P_X) as a function of the magnetic field is depicted in Figure 6c for a temperature range from 3 to 15 K, which follows a negative Brillouin-like dependence. This behavior is in contrast with undoped samples, which exhibited linear dependency[60] on the magnetic field, whereas Mn-doped samples exhibit positive P_X.[61] The bound exciton Zeeman splitting (ΔE_Z), defined as $\Delta E_Z = E_+ - E_-$ (where E_+ and E_- are the energy of σ_+ and σ_+ components, respectively), for the half-doped CdSe/CdZnS core/shell NPLs at T = 3 K is demonstrated in Figure 6d. With increasing B, ΔE_Z increases linearly and reaches a saturation point at ~ 3 T. Moreover, ΔE_Z is positive ($E_+ > E_-$), which confirms the negative circular polarization ($P_X < 0$). The same MCPL measurements were carried out for the half-doped CdSe/CdS core/shell NPLs and are shown in Figure S13. Both sets of NPLs exhibit negative Brillouin-like temperature dependence of P_X and positive saturable ΔE_Z. However, the values for P_X and ΔE_Z for CdSe/CdZnS core/shell NPLs are roughly two times higher than those of CdSe/CdS core/shell NPLs, probably due to the enhanced diffusion of the dopant ions into the better-reserved lattice of the host NPLs. The results also provide further evidence of the existence of Ag dopants with paramagnetic properties.

CONCLUSIONS

To conclude, the core/shell heterostructures of CdSe-based NPLs were successfully doped with silver through a thermodynamically controlled doping procedure. We have shown that the destruction mechanism of the NPLs in the irreversible doping regime changes from dissolution and etching, for ZnS-shelled NPLs, to fragmentation and segmentation, for CdS-shelled NPLs. The NPLs with the alloyed shell of CdZnS possess the highest resistance to high-temperature doping, with both destruction mechanisms active to a minimum extent. The emission spectra of the doped NPLs can be tuned through the doping level as long as the silver mid-gap state stays within the bandgap of the NPLs. Moreover, the recombination dynamics were shown to be sensitive to the distribution of dopant ions inside the heterostructure or on the surface, which is dependent on the composition of the shell. The silver-doped CdSe/CdZnS core/shell NPLs demonstrated superior paramagnetic properties, with P_X and ΔE_Z roughly two times higher than CdSe/CdS core/shell NPLs, which suggests lattice preservation and lattice doping of the NPLs. These findings should encourage further investigation for spintronic applications and spin-based devices based on doped CQWs where light-induced modulation of the properties is required.

ASSOCIATED CONTENT

Supporting Information

The Supporting Information is available free of charge at https://pubs.acs.org/doi/10.1021/acs.chemmater.3c00058.

Synthesis and characterization methods; additional optical characterization for the initial 4 ML CdSe core, thin core/shell, doped thin- and thick-shelled NPLs; absorption and PL evolution of core/shell samples doped at room temperature; TEM−EDS maps of Cd, Zn, S, and Ag for CdSe/ZnS NPLs; absorption spectra of doped CdSe/ZnS core/thin-shell NPLs at high temperature; PLQY of CdSe/CdZnS core/thin-shell NPLs; XRD pattern and XPS spectra of doped CdZnS-shelled NPLs; effect of OA and OLA on doping; TRF decay components before and after doping; and MCPL measurement of Ag/CdSe/CdS core/shell NPLs (PDF)

AUTHOR INFORMATION

Corresponding Author

Hilmi Volkan Demir − *UNAM-Institute of Materials Science and Nanotechnology and National Nanotechnology Research Center, Bilkent University, Ankara 06800, Turkey; LUMINOUS! Center of Excellence for Semiconductor Lighting and Displays, Singapore 639798, Singapore; Department of Electrical and Electronics Engineering, Department of Physics and Department of Physics, Bilkent University, Ankara 06800, Turkey; School of Electrical and Electronic Engineering, School of Physical and Mathematical Sciences, and School of Materials Science and Nanotechnology, Nanyang Technological University, Singapore 639798, Singapore;* orcid.org/0000-0003-1793-112X; Email: hvdemir@ntu.edu.sg, volkan@bilkent.edu.tr

Authors

Farzan Shabani − *UNAM-Institute of Materials Science and Nanotechnology and National Nanotechnology Research Center, Bilkent University, Ankara 06800, Turkey;* orcid.org/0000-0003-2174-5960

Muhammad Ahmad − *UNAM-Institute of Materials Science and Nanotechnology and National Nanotechnology Research Center, Bilkent University, Ankara 06800, Turkey*

Satish Kumar − *UNAM-Institute of Materials Science and Nanotechnology and National Nanotechnology Research Center, Bilkent University, Ankara 06800, Turkey*

Savas Delikanli − *UNAM-Institute of Materials Science and Nanotechnology and National Nanotechnology Research Center, Bilkent University, Ankara 06800, Turkey; LUMINOUS! Center of Excellence for Semiconductor Lighting and Displays, Singapore 639798, Singapore;* orcid.org/0000-0002-0613-8014

https://doi.org/10.1021/acs.chemmater.3c00058
Chem. Mater. 2023, 35, 4159−4170

Furkan Isik − *UNAM-Institute of Materials Science and Nanotechnology and National Nanotechnology Research Center, Bilkent University, Ankara 06800, Turkey;* orcid.org/0000-0001-5881-5438

Arinjoy Bhattacharya − *Department of Physics, State University of New York at Buffalo, Buffalo, New York 14260, United States;* orcid.org/0000-0002-8019-4233

Athos Petrou − *Department of Physics, State University of New York at Buffalo, Buffalo, New York 14260, United States*

Complete contact information is available at: https://pubs.acs.org/10.1021/acs.chemmater.3c00058

Author Contributions

The manuscript was written through the contributions of all authors. All authors have given approval to the final version of the manuscript.

Notes

The authors declare no competing financial interest.

■ ACKNOWLEDGMENTS

The authors gratefully acknowledge the financial support from the Agency for Science, Technology, and Research (A*STAR) MTC program, grant no M21J9b0085 (Singapore), the Ministry of Education Tier 1 grant MOE-RG62/20 (Singapore), and TUBITAK 119N343, 121N395, 20AG001, and 121C266. H.V.D. also acknowledges the support from TUBA and TUBITAK 2247-A National Leader Researchers Program (121C266).

■ REFERENCES

(1) Achtstein, A. W.; Scott, R.; Kickhöfel, S.; Jagsch, S. T.; Christodoulou, S.; Bertrand, G. H. V.; Prudnikau, A. V.; Antanovich, A.; Artemyev, M.; Moreels, I.; Schliwa, A.; Woggon, U. P-State Luminescence in CdSe Nanoplatelets: Role of Lateral Confinement and a Longitudinal Optical Phonon Bottleneck. *Phys. Rev. Lett.* **2016**, *116*, 116802.

(2) Humayun, M. H.; Hernandez-Martinez, P. L.; Gheshlaghi, N.; Erdem, O.; Altintas, Y.; Shabani, F.; Demir, H. V. Near-Field Energy Transfer into Silicon Inversely Proportional to Distance Using Quasi-2D Colloidal Quantum Well Donors. *Small* **2021**, *17*, 2103524.

(3) Rossinelli, A. A.; Rojo, H.; Mule, A. S.; Aellen, M.; Cocina, A.; De Leo, E.; Schäublin, R.; Norris, D. J. Compositional Grading for Efficient and Narrowband Emission in CdSe-Based Core/Shell Nanoplatelets. *Chem. Mater.* **2019**, *31*, 9567−9578.

(4) Han, J. H.; Kwak, M.; Kim, Y.; Cheon, J. Recent Advances in the Solution-Based Preparation of Two-Dimensional Layered Transition Metal Chalcogenide Nanostructures. *Chem. Rev.* **2018**, *118*, 6151−6188.

(5) Zhang, J.; Sun, Y.; Ye, S.; Song, J.; Qu, J. Heterostructures in Two-Dimensional CdSe Nanoplatelets: Synthesis, Optical Properties, and Applications. *Chem. Mater.* **2020**, *32*, 9490−9507.

(6) Yu, J.; Chen, R. Optical Properties and Applications of Two-Dimensional CdSe Nanoplatelets. *InfoMat* **2020**, *2*, 905−927.

(7) Delikanli, S.; Erdem, O.; Isik, F.; Dehghanpour Baruj, H.; Shabani, F.; Yagci, H. B.; Durmusoglu, E. G.; Demir, H. V. Ultrahigh Green and Red Optical Gain Cross Sections from Solutions of Colloidal Quantum Well Heterostructures. *J. Phys. Chem. Lett.* **2021**, *12*, 2177−2182.

(8) Ebrahimi, E.; Irfan, M.; Shabani, F.; Kocak, Y.; Karakurt, B.; Erdem, E.; Demir, H. V.; Ozensoy, E. Core-Crown Quantum Nanoplatelets with Favorable Type-II Heterojunctions Boost Charge Separation and Photocatalytic NO Oxidation on TiO2. *ChemCatChem* **2020**, *12*, 6329−6343.

(9) She, C.; Fedin, I.; Dolzhnikov, D. S.; Dahlberg, P. D.; Engel, G. S.; Schaller, R. D.; Talapin, D. V. Red, Yellow, Green, and Blue Amplified Spontaneous Emission and Lasing Using Colloidal CdSe Nanoplatelets. *ACS Nano* **2015**, *9*, 9475−9485.

(10) Gheshlaghi, N.; Foroutan-Barenji, S.; Erdem, O.; Altintas, Y.; Shabani, F.; Humayun, M. H.; Demir, H. V. Self-Resonant Microlasers of Colloidal Quantum Wells Constructed by Direct Deep Patterning. *Nano Lett.* **2021**, *21*, 4598−4605.

(11) Mazzaro, R.; Vomiero, A. The Renaissance of Luminescent Solar Concentrators: The Role of Inorganic Nanomaterials. *Adv. Energy Mater.* **2018**, *8*, 1801903.

(12) Delikanli, S.; Isik, F.; Shabani, F.; Baruj, H. D.; Taghipour, N.; Demir, H. V. Ultralow Threshold Optical Gain Enabled by Quantum Rings of Inverted Type-I CdS/CdSe Core/Crown Nanoplatelets in the Blue. *Adv. Opt. Mater.* **2021**, *9*, 2002220.

(13) İzmir, M.; Sharma, A.; Shendre, S.; Durmusoglu, E. G.; Sharma, V. K.; Shabani, F.; Baruj, H. D.; Delikanli, S.; Sharma, M.; Demir, H. V. Blue-Emitting CdSe Nanoplatelets Enabled by Sulfur-Alloyed Heterostructures for Light-Emitting Diodes with Low Turn-on Voltage. *ACS Appl. Nano Mater.* **2022**, *5*, 1367−1376.

(14) Rossinelli, A. A.; Riedinger, A.; Marqués-Gallego, P.; Knüsel, P. N.; Antolinez, F. V.; Norris, D. J. High-Temperature Growth of Thick-Shell CdSe/CdS Core/Shell Nanoplatelets. *Chem. Commun.* **2017**, *53*, 9938−9941.

(15) Pandya, R.; Steinmetz, V.; Puttisong, Y.; Dufour, M.; Chen, W. M.; Chen, R. Y. S.; Barisien, T.; Sharma, A.; Lakhwani, G.; Mitioglu, A.; Christianen, P. C. M.; Legrand, L.; Bernardot, F.; Testelin, C.; Chin, A. W.; Ithurria, S.; Chamarro, M.; Rao, A. Fine Structure and Spin Dynamics of Linearly Polarized Indirect Excitons in Two-Dimensional CdSe/CdTe Colloidal Heterostructures. *ACS Nano* **2019**, *13*, 10140−10153.

(16) Fan, F.; Kanjanaboos, P.; Saravanapavanantham, M.; Beauregard, E.; Ingram, G.; Yassitepe, E.; Adachi, M. M.; Voznyy, O.; Johnston, A. K.; Walters, G.; Kim, G. H.; Lu, Z. H.; Sargent, E. H. Colloidal $CdSe_{1-x}S_x$ Nanoplatelets with Narrow and Continuously-Tunable Electroluminescence. *Nano Lett.* **2015**, *15*, 4611−4615.

(17) Dufour, M.; Izquierdo, E.; Livache, C.; Martinez, B.; Silly, M. G.; Pons, T.; Lhuillier, E.; Delerue, C.; Ithurria, S. Doping as a Strategy to Tune Color of 2D Colloidal Nanoplatelets. *ACS Appl. Mater. Interfaces* **2019**, *11*, 10128−10134.

(18) Shabani, F.; Martinez, P. L. H.; Shermet, N.; Korkut, H.; Sarpkaya, I.; Dehghanpour Baruj, H.; Delikanli, S.; Isik, F.; Durmusoglu, E. G.; Demir, H. V. Gradient Type-II CdSe/CdSeTe/CdTe Core/Crown/Crown Heteronanoplatelets with Asymmetric Shape and Disproportional Excitonic Properties. *Small* **2023**, *19*, 2205729.

(19) Pinchetti, V.; Di, Q.; Lorenzon, M.; Camellini, A.; Fasoli, M.; Zavelani-Rossi, M.; Meinardi, F.; Zhang, J.; Crooker, S. A.; Brovelli, S. Excitonic Pathway to Photoinduced Magnetism in Colloidal Nanocrystals with Nonmagnetic Dopants. *Nat. Nanotechnol.* **2017**, *13*, 145−151.

(20) Wang, L.; Chen, Z.; Liang, G.; Li, Y.; Lai, R.; Ding, T.; Wu, K. Observation of a Phonon Bottleneck in Copper-Doped Colloidal Quantum Dots. *Nat. Commun.* **2019**, *10*, 4532−4538.

(21) Norris, D. J.; Efros, A. L.; Erwin, S. C. Doped Nanocrystals. *Science* **2008**, *319*, 1776−1779.

(22) Pradhan, N.; Das Adhikari, S.; Nag, A.; Sarma, D. D. Luminescence, Plasmonic, and Magnetic Properties of Doped Semiconductor Nanocrystals. *Angew. Chem., Int. Ed.* **2017**, *56*, 7038−7054.

(23) Beaulac, R.; Archer, P. I.; Ochsenbein, S. T.; Gamelin, D. R. Mn2+-Doped CdSe Quantum Dots: New Inorganic Materials for Spin-Electronics and Spin-Photonics. *Adv. Funct. Mater.* **2008**, *18*, 3873−3891.

(24) Muckel, F.; Barrows, C. J.; Graf, A.; Schmitz, A.; Erickson, C. S.; Gamelin, D. R.; Bacher, G. Current-Induced Magnetic Polarons in a Colloidal Quantum-Dot Device. *Nano Lett.* **2017**, *17*, 4768−4773.

(25) Dehnel, J.; Barak, Y.; Meir, I.; Budniak, A. K.; Nagvenkar, A. P.; Gamelin, D. R.; Lifshitz, E. Insight into the Spin Properties in

Undoped and Mn-Doped CdSe/CdS-Seeded Nanorods by Optically Detected Magnetic Resonance. *ACS Nano* **2020**, *14*, 13478−13490.
(26) Hu, R.; Wu, Z.; Zhang, Y.; Yakovlev, D. R.; Liang, P.; Qiang, G.; Guo, J.; Jia, T.; Sun, Z.; Bayer, M.; Feng, D. Long-Lived Negative Photocharging in Colloidal CdSe Quantum Dots Revealed by Coherent Electron Spin Precession. *J. Phys. Chem. Lett.* **2019**, *10*, 4994−4999.
(27) Capitani, C.; Pinchetti, V.; Gariano, G.; Santiago-González, B.; Santambrogio, C.; Campione, M.; Prato, M.; Brescia, R.; Camellini, A.; Bellato, F.; Carulli, F.; Anand, A.; Zavelani-Rossi, M.; Meinardi, F.; Crooker, S. A.; Brovelli, S. Quantized Electronic Doping towards Atomically Controlled "Charge-Engineered" Semiconductor Nanocrystals. *Nano Lett.* **2019**, *19*, 1307−1317.
(28) Buonsanti, R.; Milliron, D. J. Chemistry of Doped Colloidal Nanocrystals. *Chem. Mater.* **2013**, *25*, 1305−1317.
(29) Barrows, C. J.; Chakraborty, P.; Kornowske, L. M.; Gamelin, D. R. Tuning Equilibrium Compositions in Colloidal $Cd_{1-X}Mn_xSe$ Nanocrystals Using Diffusion Doping and Cation Exchange. *ACS Nano* **2016**, *10*, 910−918.
(30) Knowles, K. E.; Hartstein, K. H.; Kilburn, T. B.; Marchioro, A.; Nelson, H. D.; Whitham, P. J.; Gamelin, D. R. Luminescent Colloidal Semiconductor Nanocrystals Containing Copper: Synthesis, Photophysics, and Applications. *Chem. Rev.* **2016**, *116*, 10820−10851.
(31) Jawaid, A. M.; Chattopadhyay, S.; Wink, D. J.; Page, L. E.; Snee, P. T. Cluster-Seeded Synthesis of Doped CdSe:Cu4 Quantum Dots. *ACS Nano* **2013**, *7*, 3190−3197.
(32) Vlaskin, V. A.; Barrows, C. J.; Erickson, C. S.; Gamelin, D. R. Nanocrystal Diffusion Doping. *J. Am. Chem. Soc.* **2013**, *135*, 14380−14389.
(33) Lee, W.; Oh, J.; Kwon, W.; Lee, S. H.; Kim, D.; Kim, S. Synthesis of Ag/Mn Co-Doped CdS/ZnS (Core/Shell) Nanocrystals with Controlled Dopant Concentration and Spatial Distribution and the Dynamics of Excitons and Energy Transfer between Co-Dopants. *Nano Lett.* **2019**, *19*, 308−317.
(34) Ott, F. D.; Spiegel, L. L.; Norris, D. J.; Erwin, S. C. Microscopic Theory of Cation Exchange in CdSe Nanocrystals. *Phys. Rev. Lett.* **2014**, *113*, 156803−156805.
(35) Lesnyak, V.; Brescia, R.; Messina, G. C.; Manna, L. Cu Vacancies Boost Cation Exchange Reactions in Copper Selenide Nanocrystals. *J. Am. Chem. Soc.* **2015**, *137*, 9315−9323.
(36) Zhang, J.; Di, Q.; Liu, J.; Bai, B.; Liu, J.; Xu, M.; Liu, J. Heterovalent Doping in Colloidal Semiconductor Nanocrystals: Cation-Exchange-Enabled New Accesses to Tuning Dopant Luminescence and Electronic Impurities. *J. Phys. Chem. Lett.* **2017**, *8*, 4943−4953.
(37) Chen, D.; Viswanatha, R.; Ong, G. L.; Xie, R.; Balasubramaninan, M.; Peng, X. Temperature Dependence of "Elementary Processes" in Doping Semiconductor Nanocrystals. *J. Am. Chem. Soc.* **2009**, *131*, 9333−9339.
(38) Khan, A. H.; Pinchetti, V.; Tanghe, I.; Dang, Z.; Martín-García, B.; Hens, Z.; Van Thourhout, D.; Geiregat, P.; Brovelli, S.; Moreels, I. Tunable and Efficient Red to Near-Infrared Photoluminescence by Synergistic Exploitation of Core and Surface Silver Doping of CdSe Nanoplatelets. *Chem. Mater.* **2019**, *31*, 1450−1459.
(39) Erwin, S. C.; Zu, L.; Haftel, M. I.; Efros, A. L.; Kennedy, T. A.; Norris, D. J. Doping Semiconductor Nanocrystals. *Nature* **2005**, *436*, 91−94.
(40) Liu, J.; Zhao, Q.; Liu, J. L.; Wu, Y. S.; Cheng, Y.; Ji, M. W.; Qian, H. M.; Hao, W. C.; Zhang, L. J.; Wei, X. J.; Wang, S. G.; Zhang, J. T.; Du, Y.; Dou, S. X.; Zhu, H. S. Heterovalent-Doping-Enabled Efficient Dopant Luminescence and Controllable Electronic Impurity Via a New Strategy of Preparing II-VI Nanocrystals. *Adv. Mater.* **2015**, *27*, 2753−2761.
(41) Viswanatha, R.; Brovelli, S.; Pandey, A.; Crooker, S. A.; Klimov, V. I. Copper-Doped Inverted Core/Shell Nanocrystals with "Permanent" Optically Active Holes. *Nano Lett.* **2011**, *11*, 4753−4758.
(42) Bai, B.; Xu, M.; Li, J.; Zhang, S.; Qiao, C.; Liu, J.; Zhang, J. Dopant Diffusion Equilibrium Overcoming Impurity Loss of Doped QDs for Multimode Anti-Counterfeiting and Encryption. *Adv. Funct. Mater.* **2021**, *31*, 2100286−2100287.
(43) Sharma, M.; Gungor, K.; Yeltik, A.; Olutas, M.; Guzelturk, B.; Kelestemur, Y.; Erdem, T.; Delikanli, S.; McBride, J. R.; Demir, H. V. Near-Unity Emitting Copper-Doped Colloidal Semiconductor Quantum Wells for Luminescent Solar Concentrators. *Adv. Mater.* **2017**, *29*, 1700821−1700910.
(44) Shabani, F.; Dehghanpour Baruj, H.; Yurdakul, I.; Delikanli, S.; Gheshlaghi, N.; Isik, F.; Liu, B.; Altintas, Y.; Canımkurbey, B.; Demir, H. V. Deep-Red-Emitting Colloidal Quantum Well Light-Emitting Diodes Enabled through a Complex Design of Core/Crown/Double Shell Heterostructure. *Small* **2022**, *18*, 2106115.
(45) Hu, S.; Shabani, F.; Liu, B.; Zhang, L.; Guo, M.; Lu, G.; Zhou, Z.; Wang, J.; Huang, J. C.; Min, Y.; Xue, Q.; Demir, H. V.; Liu, C. High-Performance Deep Red Colloidal Quantum Well Light-Emitting Diodes Enabled by the Understanding of Charge Dynamics. *ACS Nano* **2022**, *16*, 10840−10851.
(46) Polovitsyn, A.; Dang, Z.; Movilla, J. L.; Martín-García, B.; Khan, A. H.; Bertrand, G. H. V.; Brescia, R.; Moreels, I. Synthesis of Air-Stable CdSe/ZnS Core-Shell Nanoplatelets with Tunable Emission Wavelength. *Chem. Mater.* **2017**, *29*, 5671−5680.
(47) Yang, L.; Knowles, K. E.; Gopalan, A.; Hughes, K. E.; James, M. C.; Gamelin, D. R. One-Pot Synthesis of Monodisperse Colloidal Copper-Doped CdSe Nanocrystals Mediated by Ligand-Copper Interactions. *Chem. Mater.* **2016**, *28*, 7375−7384.
(48) Abbaschian, R.; Reed-Hill, R. E. *Physical Metallurgy Principles—SI Version*; Cengage Learning, 2009.
(49) Hazarika, A.; Fedin, I.; Hong, L.; Guo, J.; Srivastava, V.; Cho, W.; Coropceanu, I.; Portner, J.; Diroll, B. T.; Philbin, J. P.; Rabani, E.; Klie, R.; Talapin, D. V. Colloidal Atomic Layer Deposition with Stationary Reactant Phases Enables Precise Synthesis of "Digital" II−VI Nano-Heterostructures with Exquisite Control of Confinement and Strain. *J. Am. Chem. Soc.* **2019**, *141*, 13487−13496.
(50) Altintas, Y.; Liu, B.; Hernández-Martínez, P. L.; Gheshlaghi, N.; Shabani, F.; Sharma, M.; Wang, L.; Sun, H.; Mutlugun, E.; Demir, H. V. Spectrally Wide-Range-Tunable, Efficient, and Bright Colloidal Light-Emitting Diodes of Quasi-2D Nanoplatelets Enabled by Engineered Alloyed Heterostructures. *Chem. Mater.* **2020**, *32*, 7874−7883.
(51) Wang, D.; Xie, T.; Peng, Q.; Li, Y. Ag, Ag2S, and Ag2Se Nanocrystals: Synthesis, Assembly, and Construction of Mesoporous Structures. *J. Am. Chem. Soc.* **2008**, *130*, 4016−4022.
(52) Kim, T.; Park, J.; Hong, Y.; Oh, A.; Baik, H.; Lee, K. Janus to Core−Shell to Janus: Facile Cation Movement in $Cu_{2-x}S/Ag_2S$ Hexagonal Nanoplates Induced by Surface Strain Control. *ACS Nano* **2019**, *13*, 11834−11842.
(53) Du, Y.; Xu, B.; Fu, T.; Cai, M.; Li, F.; Zhang, Y.; Wang, Q. Near-Infrared Photoluminescent Ag2S Quantum Dots from a Single Source Precursor. *J. Am. Chem. Soc.* **2010**, *132*, 1470−1471.
(54) Hinterding, S. O. M.; Salzmann, B. B. V.; Vonk, S. J. W.; Vanmaekelbergh, D.; Weckhuysen, B. M.; Hutter, E. M.; Rabouw, F. T. Single Trap States in Single CdSe Nanoplatelets. *ACS Nano* **2021**, *15*, 7216−7225.
(55) Boles, M. A.; Ling, D.; Hyeon, T.; Talapin, D. V. The Surface Science of Nanocrystals. *Nat. Mater.* **2016**, *15*, 141−153.
(56) Galle, T.; Kazes, M.; Hübner, R.; Lox, J.; Samadi Khoshkhoo, M.; Sonntag, L.; Tietze, R.; Sayevich, V.; Oron, D.; Koitzsch, A.; Lesnyak, V.; Eychmüller, A. Colloidal Mercury-Doped CdSe Nanoplatelets with Dual Fluorescence. *Chem. Mater.* **2019**, *31*, 5065−5074.
(57) Ali, F.; Das, S.; Banerjee, S.; Maddala, B. G.; Rana, G.; Datta, A. Intense Photoluminescence from Cu-Doped CdSe Nanotetrapods Triggered by Ultrafast Hole Capture. *Nanoscale* **2021**, *13*, 14228−14235.
(58) Chestnoy, N.; Harris, T. D.; Hull, R.; Brus, L. E. Luminescence and Photophysics of Cadmium Sulfide Semiconductor Clusters: The Nature of the Emitting Electronic State. *J. Phys. Chem.* **1986**, *90*, 3393−3399.
(59) Stroyuk, O.; Raevskaya, A.; Gaponik, N.; Selyshchev, O.; Dzhagan, V.; Schulze, S.; Zahn, D. R. T. Origin of the Broadband

https://doi.org/10.1021/acs.chemmater.3c00058
Chem. Mater. 2023, 35, 4159−4170

Photoluminescence of Pristine and Cu^+/Ag^+-Doped Ultrasmall CdS and CdSe/CdS Quantum Dots. *J. Phys. Chem. C* **2018**, *122*, 10267−10277.
(60) Najafi, A.; Sharma, M.; Delikanli, S.; Bhattacharya, A.; Murphy, J. R.; Pientka, J.; Sharma, A.; Quinn, A. P.; Erdem, O.; Kattel, S.; Kelestemur, Y.; Kovalenko, M. V.; Rice, W. D.; Demir, H. V.; Petrou, A. Light-Induced Paramagnetism in Colloidal Ag^+-Doped CdSe Nanoplatelets. *J. Phys. Chem. Lett.* **2021**, *12*, 2892−2899.
(61) Shornikova, E. V.; Yakovlev, D. R.; Tolmachev, D. O.; Ivanov, V. Y.; Kalitukha, I. V.; Sapega, V. F.; Kudlacik, D.; Kusrayev, Y. G.; Golovatenko, A. A.; Shendre, S.; Delikanli, S.; Demir, H. V.; Bayer, M. Magneto-Optics of Excitons Interacting with Magnetic Ions in CdSe/CdMnS Colloidal Nanoplatelets. *ACS Nano* **2020**, *14*, 9032−9041.

https://doi.org/10.1021/acs.chemmater.3c00058
Chem. Mater. 2023, 35, 4159−4170